Periodic perturbation of one of two identical chemical oscillators coupled via inhibition

Vladimir K. Vanag and Irving R. Epstein
Department of Chemistry, MS 015, Brandeis University, Waltham, Massachusetts 02454, USA
(Received 11 January 2010; published 23 June 2010)

We study perturbation with period T_p of one of two model Belousov-Zhabotinsky chemical oscillators diffusively coupled through an inhibitory species. We find a variety of resonance regimes, characterized as $N_1:N_2:n$, where N_1 (N_2) and n are the numbers of spikes of the perturbed (unperturbed) oscillator and the external perturbation, respectively, per global period T_G. The resonance mode is determined primarily by the ratios T_p/T_0 and T_p/T_C, where T_0 and T_C are the periods of a single oscillator and of two coupled antiphase oscillators, respectively ($T_C \cong 2T_0$ at large coupling strength). The period of the perturbed oscillator can be tuned over a wide range (from T_0 to $>10T_0$) by varying T_p between T_C and T_0.

DOI: 10.1103/PhysRevE.81.066213 PACS number(s): 82.40.Bj, 82.20.Wt, 05.45.Xt

I. INTRODUCTION

Coupled and periodically forced oscillators continue to attract the attention of investigators in many areas of physics, chemistry, and biology [1–5]. It is well known that a pair of coupled oscillators can generate a variety of behaviors including in-phase and antiphase oscillations, phase death, and multistability (birhythmicity) [6–10]. Periodic perturbation of a single oscillator is associated with such well-known phenomena as resonance, Arnol'd tongues, and devil's staircases [11–16].

In early experimental studies of coupled chemical oscillators, the coupling is typically established by direct mass exchange between cells, so that both activator (a species whose concentration grows autocatalytically) and inhibitor (a species that prevents autocatalysis) participate in the coupling. Coupling by activator or inhibitor alone, however, can give different behavior. When the coupling is purely excitatory (via the activator) or when excitatory coupling is dominant [17,18], a system typically has two states: an asynchronous mode, in which the oscillators have random phases, and a synchronous regime, where the coupling strength is above some critical value and all oscillators are in-phase or almost in-phase with one another. Inhibitory coupling (sometimes called repulsive coupling), which has been much less investigated, generally yields a richer variety of synchronous regimes and multistability between them [19–23]. An important example, in which inhibitory coupling is often dominant, is interneuron communication in the brain [24].

Recently, we developed an experimental system consisting of a linear array of small (50–300 μm in diameter) identical water droplets separated by oil gaps [25]. Each drop contains the reactants of the oscillatory Belousov-Zhabotinsky (BZ) reaction [26,27]: malonic acid (MA), bromate, sulfuric acid, ferroin (catalyst), and a small amount of ruthenium trisbipyridyl [$Ru(bpy)_3$], which serves both as a cocatalyst and to make the BZ reaction photosensitive. These BZ droplets are diffusively coupled through the inhibitor, Br_2, which preferentially dissolves in the oil gaps. We observed antiphase synchronization and stationary Turing patterns in this system [25], both of which indicate inhibitory coupling between BZ droplets.

To create a simple caricature of a neural system using such inhibitorily coupled BZ drops, we need to introduce some inputs that mimic those received by sensory neurons. The simplest way to do this is by periodic forcing of a subset of the BZ drops, e.g., by illumination through a mask. In general, one might perturb different drops at different frequencies. To gain initial insight into this potentially very complex experimental system, we investigate here theoretically the simplest such configuration, namely, two inhibitorily and diffusively coupled BZ oscillators subjected to periodic illumination of one of them. Note that periodic illumination of a single oscillator can be viewed as unidirectional coupling of two oscillators, which occurs in neurons with chemical inhibitory synapses [24].

II. MODEL

As our model for a single BZ oscillator, we use a recently developed four-variable scheme [28] deduced from the Field-Körös-Noyes (FKN) model of the BZ reaction [29], the behavior of which in a relatively small water droplet can be accurately described by ordinary differential equations (ODEs). We consider a circular coupling arrangement: drop_1-oil_12-drop_2-oil_21-drop_1. We thus have two identical oil gaps between drops. Since we describe diffusive coupling in terms of ODE (see Appendix A), our full model of two coupled oscillators with perturbation $P_1(t)$ of droplet 1 reads

$$dx_1/dt = -k_1x_1y_1 + k_2y_1 - 2k_3x_1^2 + k_4x_1(c_0 - z_1)/(c_0 - z_1 + c_{min}), \quad (1)$$

$$dy_1/dt = -3k_1x_1y_1 - 2k_2y_1 - k_3x_1^2 + k_7u_1 + k_9z_1 + P_1(t), \quad (2)$$

$$dz_1/dt = 2k_4x_1(c_0 - z_1)/(c_0 - z_1 + c_{min}) - k_9z_1 - k_{10}z_1 + P_1(t), \quad (3)$$

$$du_1/dt = 2k_1x_1y_1 + k_2y_1 + k_3x_1^2 - k_7u_1 - 2k_fu_1 + k_b(s_{12} + s_{21})/r_V, \quad (4)$$

$$ds_{12}/dt = r_Vk_fu_1 - 2k_bs_{12} + r_Vk_fu_2, \quad (5)$$

$$ds_{21}/dt = r_V k_f u_1 - 2k_b s_{21} + r_V k_f u_2, \quad (5')$$

$$du_2/dt = 2k_1 x_2 y_2 + k_2 y_2 + k_3 x_2^2 - k_7 u_2 - 2k_f u_2 + k_b(s_{12} + s_{21})/r_V, \quad (6)$$

$$dx_2/dt = -k_1 x_2 y_2 + k_2 y_2 - 2k_3 x_2^2 + k_4 x_2 (c_0 - z_2)/(c_0 - z_2 + c_{min}), \quad (7)$$

$$dy_2/dt = -3k_1 x_2 y_2 - 2k_2 y_2 - k_3 x_2^2 + k_7 u_2 + k_9 z_2, \quad (8)$$

$$dz_2/dt = 2k_4 x_2 (c_0 - z_2)/(c_0 - z_2 + c_{min}) - k_9 z_2 - k_{10} z_2, \quad (9)$$

where $x=[X]=[HBrO_2]$ (activator), $y=[Y]=[Br^-]$ (inhibitor), $u=[U]=[Br_2]$ (inhibitor), $z=[Z]$ (oxidized form of the catalyst), and s_{12} and s_{21} are $[Br_2]$ in the oil gaps between water droplets 1 and 2. Variables s_{12} and s_{21} are equal to each other and one of these two variables can be easily eliminated by, for example, summation of Eqs. (5) and (5′) and introducing a new variable $s \equiv s_{12}+s_{21}$. This means that there is no difference between periodic (circular) and no-flux boundary conditions in this special case of two coupled oscillators. We prefer to keep both variables s_{12} and s_{21} as well as Eqs. (5) and (5′) since this form is easily extendable for three or more BZ drops linearly or circularly coupled through oil gaps. Subindices 1 and 2 refer variables x, y, z, and u to water droplets 1 and 2, respectively,

$$P_1(t) = A(t) \times (c_0 - z_1)/(b_C/b + 1), \quad (10)$$

where $A(t)=A$ if $[\sin(2\pi t/T_P)-0.5]>0$ (A is the strength of the perturbation measured in s^{-1}) and $A(t)=0$ otherwise; T_P is the period of the square wave perturbation; for the chosen signal, $P_1(t)$, the ratio between the intervals when $A(t)=A$ and when $A(t)=0$ is 1:2; note that $P_1(t)$ depends on z_1, the concentration of the oxidized form of the catalyst, which serves as an antenna for light ($\lambda_{max}=450$ nm). The square perturbation is chosen here to correspond to the waveform often used in experiments forced by light, where a diaphragm is periodically open and closed. The time-averaged signal, $\langle P_1(t)\rangle$, is positive; periodic forcing $P_1(t)$ at sufficiently high frequency acts like constant illumination with amplitude $A/3$. The constants c_0, b, and b_C in Eq. (10) are the total (reduced+oxidized forms) concentration of the catalyst (c_0), the concentration of bromomalonic acid (b), and $0.05M$ [30], respectively. The term $(b_C/b+1)$ in Eq. (10) originates from the competition between two reactions: internal quenching of the photoexcited state of the ruthenium complex $[Ru(bpy)_3^{2+}]^*$ and reaction between $[Ru(bpy)_3^{2+}]^*$ and bromomalonic acid [30].

The coupling strength k_f is approximately equal to D/l_d^2 (if $P_K r_V > 1$, see Appendix A), where l_d is the droplet size and D is the diffusion coefficient of Br_2 in water and in oil (which we take to be roughly equal); $k_b = r_V k_f / P_K$, P_K is the partition coefficient between oil and water for Br_2; $r_V = V_W/V_{oil}$ is the volume ratio of the water droplet and the oil gap. In the case of one-dimensional (1D) (D=dimensional) droplets (e.g., in a capillary), $r_V = l_d/l_g$, where l_g is the length of the gap. In Appendix A we show how the diffusive coupling can be described by ODE and find the dependences of k_f and k_b on l_d, l_g, and P_K.

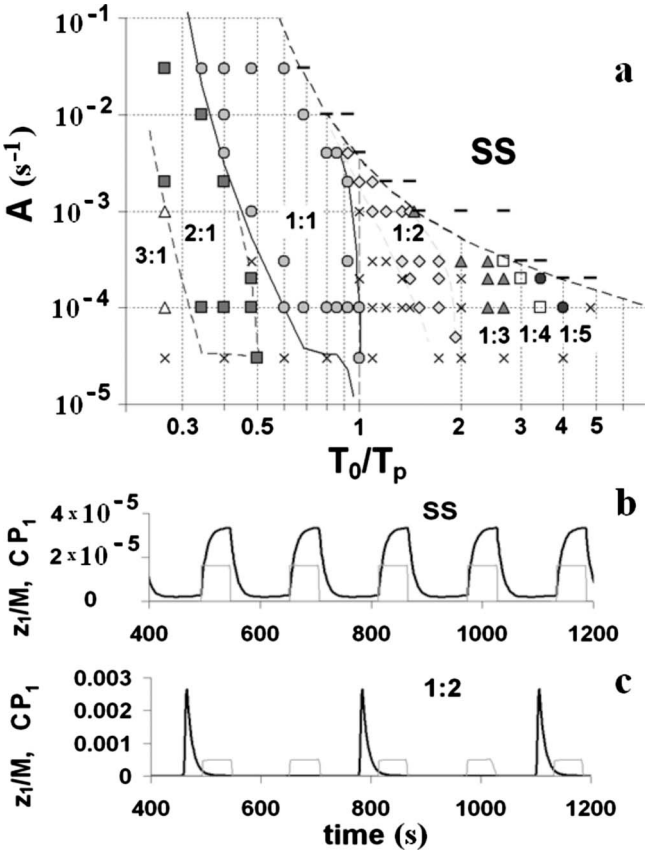

FIG. 1. (a) Phase diagram showing the response of a single BZ oscillator to periodic perturbation with amplitude A and period T_P in models (1)–(4). $T_0=240$ s is the period of the unperturbed BZ oscillator. Resonance regions N_1: n, where N_1 and n are the numbers of the BZ and external oscillations, respectively, per global period, are marked. Symbols: (SS), suppressed state; ●, resonance 1:5; □, 1:4; dark triangles, 1:3; ◇, 1:2; gray circles, 1:1; dark squares, 2:1; △, 3:1, x, other resonances. Constant illumination suppresses oscillations at an amplitude of 2.9×10^{-5}, which corresponds to $A=8.7\times10^{-5}$ for periodic forcing at high frequencies. Constants: $k_1=k_1'h$, $k_1'/(M^{-2}\,s^{-1})=2\times10^6$, $k_2=k_2'h^2a$, $k_2'/(M^{-3}\,s^{-1})=2$, $k_3'/(M^{-1}\,s^{-1})=3000$, $k_4=k_4'ha$, $k_4'/(M^{-2}\,s^{-1})=42$, $k_5=k_5'h$, $k_5'/(M^{-2}\,s^{-1})=5\times10^9$, $k_7=k_7'm$, $k_7'/(M^{-1}\,s^{-1})=29$, $k_r/(M^{-1}\,s^{-1})=2\times10^8$, $k_{red}/(M^{-1}\,s^{-1})=5\times10^6$, $k_9=k_9'm$, $k_9'=0.12\ M^{-1}\,s^{-1}$, $k_{10}=k_{10}'m$, and $k_{10}'/(M^{-1}\,s^{-1})=0.05$. (b) and (c) Kinetic curves (note the difference in scale) at $T_P=160$ s and $A/s^{-1}=$(b) 2×10^{-3} and (c) 3×10^{-4} showing two regimes, SS and 1:2, respectively. Periodic signal $P_1(t)$ is seen as a square wave. Coefficient $C/(M/s)=$(b) 5 and (c) 1000. Note that if the scale in (b) were the same as in (c), there would be no visible oscillations in (b).

In models (1)–(9), the concentrations of the BZ reactants, $m=[MA]$, $b=0.1m$, $a=[BrO_3^-]$, $h=[H^+]$, are incorporated into the rate constants k_1-k_{10} (see caption to Fig. 1) and kept unchanged throughout the paper as $h=0.15M$, $a=0.3M$, $m=0.6M$, and $c_0=0.003M$ (if other values are not specified), $c_{min}=[2k_r(k_9+k_{10})c_0]^{0.5}/k_{red}$. The concentrations h, a, m, and c_0 are chosen in such a way that the period of a single oscillator remains almost unchanged when we intro-

duce the variables s_{12} and s_{21} without the second oscillator at any constants k_f and k_b used in this work. In other words, the coupling of a BZ drop to the oil gap does not significantly affect our BZ oscillator. In our simulations we focus on the effects of varying the parameters of periodic perturbation (A, T_p) and coupling (k_f, k_b).

III. PERIODIC PERTURBATION OF A SINGLE OSCILLATOR

Before analyzing the full models (1)–(9), we investigate the dependence of the response of a single oscillator, Eqs. (1)–(4) with $k_f=0$, on the period T_P and amplitude A of perturbation. The behavior of the system is shown in the phase diagram in Fig. 1(a), where we see a number of resonances that resemble Arnol'd tongues. The only exception is the area marked SS, where oscillations are suppressed [shown in Fig. 1(b)]. This behavior arises from the fact that $\langle P_1(t)\rangle > 0$. Note that at our parameters the BZ oscillations normally have amplitude close to c_0. We refer to the oscillations being "suppressed" when they cannot be observed experimentally, i.e., when their amplitude is at least two orders of magnitude less than c_0. As the perturbing amplitude A increases, the weaker resonances such as $N_1:n=1:5, 1:4, 1:3, 1:2$ [shown in Fig. 1(c)] die first, where N_1 and n are the numbers of BZ spikes and oscillations of $P_1(t)$, respectively, per global period T_G. The value of T_G can be used to determine n and the average period T_{1_av} of the BZ oscillations as $n=T_G/T_P$ and $T_{1\_av}=nT_P/N_1$.

If we make a horizontal cross section of the phase diagram in Fig. 1 at a relatively small amplitude, for example at $A=10^{-4}$, we obtain the devil's staircase shown in Fig. 2(a). However, as we shall see later, it is more convenient to present the same cross section in terms of T_{1_av} and T_P, which we do in Fig. 2(b) in the normalized coordinates T_{1_av}/T_0-T_P/T_0. Because of the shape of this function, we shall refer to it as a set of "sheaf resonances." The slope of the segment (shown by dotted lines) corresponding to the resonance $N_1:n$ is n/N_1.

IV. TWO INHIBITORILY COUPLED BZ OSCILLATORS WITHOUT PERTURBATION

Consider now model (1)–(9) at $P_1(t)=0$, i.e., without perturbation. In general, there are several possible dynamical regimes for such a configuration (see Fig. 3): (i) in-phase and (ii) antiphase oscillations; (iii) a Turing stationary mode, in which one oscillator is close to the fully oxidized state while the other is close to the fully reduced state; and three additional modes at relatively large time delay (small k_b): (iv) one oscillator exhibits large amplitude oscillations (with the amplitude of z close to c_0) and the other shows small-amplitude oscillations (less than $0.01c_0$), i.e., suppressed oscillations; (v) a chaoticlike mode at still smaller k_b, in which both oscillators demonstrate alternating bursting with different numbers of spikes in each burst; this mode can be considered as a variant of mode (iv) in which two oscillators (with large and small amplitudes) alternate, (vi) oscillator death, a mode in which both oscillators are in the same steady state (we did not observe this mode in our simulations but theoretically such a mode is possible [31]).

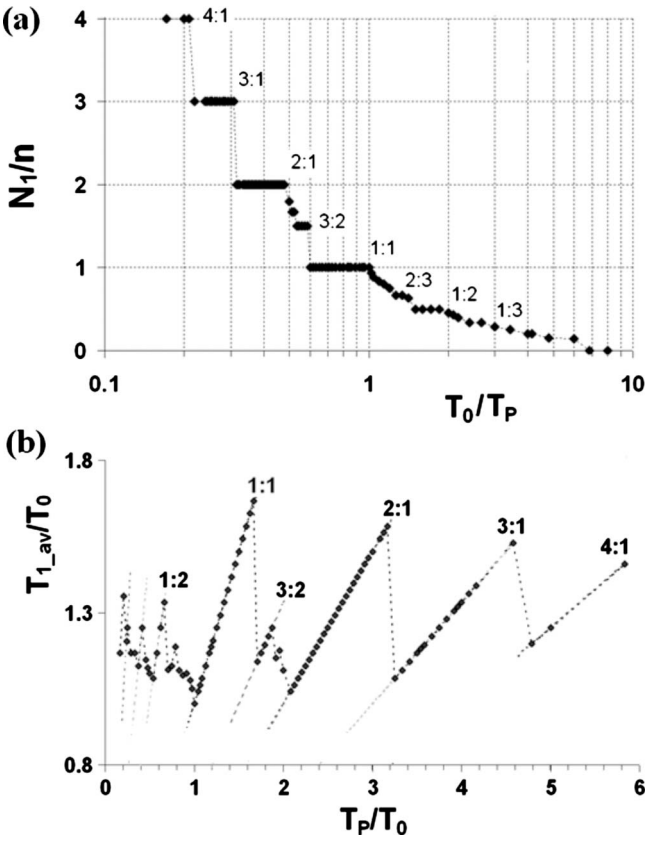

FIG. 2. (a) Devil's staircase showing N_1/n as a function of T_0/T_P for a single BZ oscillator [model (1)–(4)] subject to periodic perturbation $P(t)$ with period T_P and amplitude $A=10^{-4}$ s^{-1}. Period of the unperturbed system $T_0=240$ s. (b) Sheaf resonances corresponding to (a), but in coordinates, T_{1_av}/T_0-T_P/T_0, where $T_{1\_av}=nT_P/N_1$.

For our chosen concentrations, which lie well within the oscillatory domain for a single oscillator, and for small time delay, k_b^{-1}, we typically observe only in-phase or antiphase oscillations. The in-phase oscillations, which have a relatively small basin of attraction, have the same oscillation period as a single unperturbed oscillator, T_0, at all coupling strengths. The period of antiphase oscillations, T_C, depends on the coupling strength k_f. In Fig. 4, we show the dependence of T_C on k_f for several sets of model parameters. We see that the function $T_C(k_f)$ has a sigmoidal shape in coordinates $T_C-\log(k_f)$, with an inflection point in the range $k_f=0.1-1$ s^{-1}. The position of the inflection point depends primarily on the concentration of MA: the smaller m, the smaller $k_{f\_inflection}$. The maximum value of T_C at the largest k_f is close to $2T_0$. The presence of two periods of oscillation, T_C and T_0, is important for the behavior of the system under periodic perturbation.

V. RESULTS: PERIODIC FORCING

In the presence of periodic forcing, oscillator 1 is subject to two periodic signals: external periodic forcing $P_1(t)$ with

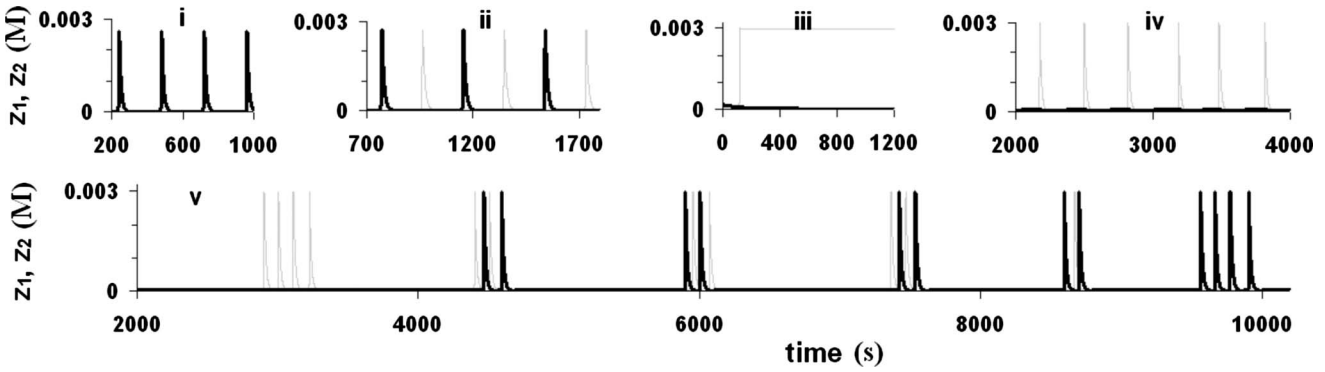

FIG. 3. Dynamical regimes for two inhibitorily coupled BZ oscillators [models (1)–(9)]. (i) and (ii) $h=0.15M$, $a=0.3M$, $m=0.6M$, $k_f=1\ s^{-1}$, $P_K=2.5$, and $r_V=20$; (iii) $m=0.05$, $k_f=10\ s^{-1}$, h,a,P_K, and r_V as in (i); (iv) $h=0.3M$, $m=0.5M$, $P_K=10$, $r_V=0.01$, a, and k_f as in (i); (v) $r_V=0.002$, h, m, P_K, a, and k_f as in (iv). Other parameters as in Fig. 1.

period T_P and periodic forcing by coupled oscillator 2, which has its own period of oscillation, T_0, if alone. In the case of strong coupling (large k_f) and relatively small forcing amplitude, A, it is more appropriate to consider resonance between the periods T_P and T_C. The interplay between T_P and T_0 or between T_P and T_C can be rather complex, leading to resonances that can be characterized by ratios $N_1:N_2:n$, where N_1 (N_2) and n are the numbers of spikes of oscillator 1 (2) and the external perturbation, respectively, per global period $T_G=nT_P$. In Fig. 5, we present coarse-grained diagrams showing the major resonances in the planes T_0/T_P-A and T_P/T_C-k_f. In Fig. 5(a), we see five regimes that survive at large amplitude A: 2:2:1, 1:2:1, 1:1:1, 0:1:1, and $0:0:n$, and three additional regimes at smaller A: 1:2:2, 1:1:2, and 0:1:2. The mode $0:0:n$ signifies that both oscillators 1 and 2 are suppressed (they oscillate with very small amplitude, similar to the behavior shown in Fig. 1(b). In some sense, this regime corresponds to SS in Fig. 1. In Fig. 5(b), we show the basins of attraction for several resonances as a function of k_f. Resonance $0:0:n$ requires relatively large k_f.

If we make a horizontal cross section of the diagram in Fig. 5(a) at large A (e.g., $A=5\times10^{-2}$), we obtain the following sequence of regimes: 2:2:1, 1:2:1, 1:1:1, 0:1:1, and $0:0:n$. In Fig. 6, we present such a cross-section in two pairs of planes, N_1/n (N_2/n)-T_0/T_P and T_{1_av}/T_0 (T_{2_av}/T_0)-T_P/T_0. The dependences of N_1/n and N_2/n on T_0/T_P [Fig. 6(a) similar to Fig. 2(a)] form a doubled devil's staircase. As is seen in Fig. 6(b) [which is similar to Fig. 2(b)], the average periods $T_{1\_av}(=T_G/N_1)$ and $T_{2\_av}(=T_G/N_2)$ increase linearly with T_P in each resonance range and then either jump down or continue increasing in the domain of another resonance. Almost all the points in Fig. 6(b) lie on straight lines with

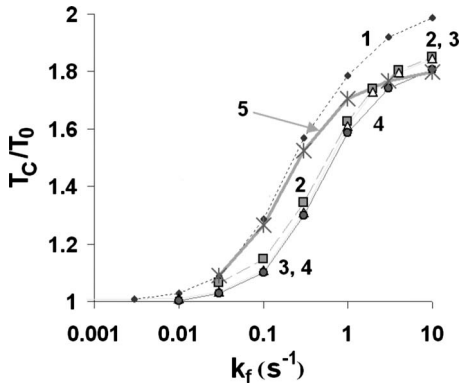

FIG. 4. Period T_C of antiphase oscillations for two coupled BZ oscillators as a function of coupling strength k_f. For curve 1 ($T_0=1026$ s), $h=0.1M$, $a=0.15M$, and $m=0.2M$. For curve 5 ($T_0=278$ s), $h=0.15M$, $a=0.3M$, and $m=0.2M$. For curves (2)–(4) ($T_0=240$ s), $h=0.15M$, $a=0.3M$, and $m=0.6M$. For curve 2, $P_K=2.5$, $r_V=1$; for curve 3, $P_K=0.125$, $r_V=1$; for curves 1, 4, and 5, $P_K=2.5$, $r_V=2$.

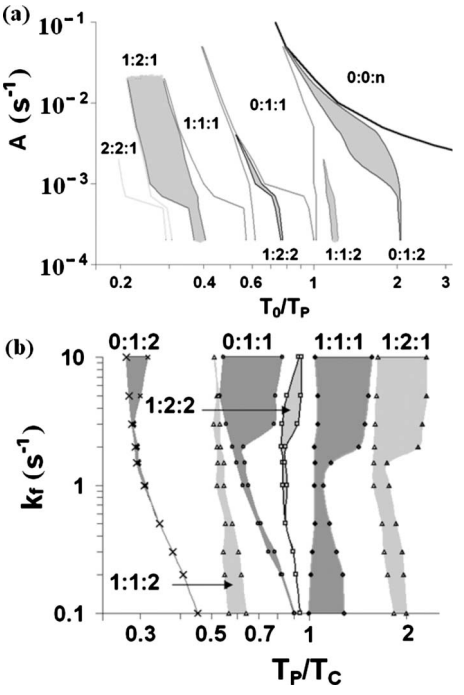

FIG. 5. Major resonances for two coupled BZ oscillators subject to periodic perturbation (period T_P) of oscillator 1 (a) in the T_0/T_P-A plane ($T_0=240$ s) at coupling strength $k_f=1$, (b) in the T_P/T_C-k_f plane at $A=5\times10^{-4}\ s^{-1}$ (T_C depends on k_f as in Fig. 4). Resonances are marked as $N_1:N_2:n$, where N_1 (N_2) and n are, respectively, the numbers of spikes of oscillator 1 (2) and the external perturbation per global period $T_G=nT_P$. Parameters of model (1)–(9): $h=0.15$, $a=0.3$, $m=0.6$, $c_0=0.003$, $k_b=r_Vk_f/P_K$, for (a) $P_K=2.5$, $r_V=2$, for (b) $P_K=0.125$, $r_V=1$.

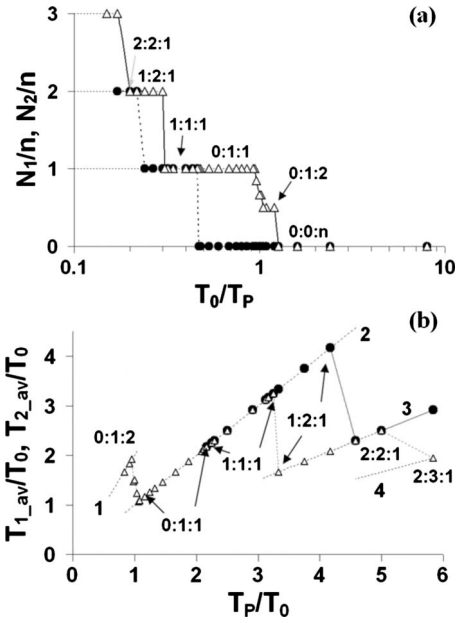

FIG. 6. (a) Doubled devil's staircase showing dependence of ratios N_1/n (black circles) and N_2/n (open triangles) on T_0/T_P (T_0=240 s) in models (1)–(9) with k_f=1 s^{-1} and periodic perturbation $P_1(t)$ of oscillator 1 with period T_P and amplitude A =10^{-2} s^{-1}. (b) Sheaf resonances. The same result as in (a), but in coordinates T_{1_av}/T_0-T_P/T_0 and T_{2_av}/T_0-T_P/T_0, where T_{1_av} =nT_P/N_1 and T_{2_av}=nT_P/N_2. Parameters as in Fig. 5. Slopes of lines 1, 2, 3, and 4 are 2, 1, 1/2, and 1/3, respectively.

slopes 2, 1, 1/2, and 1/3. Average periods T_{1_av} and T_{2_av} belonging to different resonances may lie on the same curve. For example, curve 2 with a slope of 1 contains points from resonances 0:1:1, 1:1:1, and 1:2:1. For this reason, a sheaf resonance plot may be more informative than a devil's staircase.

The resonances shown in Fig. 5 have the following features. The average period of the illuminated oscillator, T_{1_av}, is always greater than or equal to the average period of the unperturbed oscillator, T_{2_av}, or equivalently, $N_2 \geq N_1$ (see Fig. 6). At large frequency T_P^{-1} and amplitude A, both oscillators 1 and 2 are suppressed (regime $0:0:n$). At moderate T_P^{-1} and A, only oscillator 1 is suppressed (only regimes 0:1:1 and 0:1:2 are shown in Fig. 5, though other regimes $0:N_1:n$ also exist). At small T_P^{-1} and relatively large $A(>10^{-3})$ regimes $N_1:N_2=1:1$ and $N_1:N_2=1:2$ alternate. At smaller A, there are many other regimes, one of which (when $T_0<T_P<T_C$) we study more carefully below.

The resonances 0:1:1, 0:1:2, $0:1:n$, when oscillator 1 is suppressed, correspond to periods $T_P=T_0$, $T_P=T_0/2$, and T_P =T_0/n, respectively, at small A. The resonances 1:1:2, 1:1:1, and 2:2:1, when $N_1=N_2$, correspond to periods $T_P \cong T_C/2$, $T_P \cong T_C$, and $T_P \cong 2T_C$, respectively, at small A ($T_C \cong 386$ s at k_f=1 s^{-1} and $T_C/T_0 \cong 1.6$). Resonances 1:2:2 and 1:2:1 (when $N_1=2N_2$) correspond to periods $T_P \cong 0.75T_C$ and T_P $\cong 1.5T_C$, respectively, at small A. The transition point from "small A" to "large A" depends on the coupling strength k_f and can be estimated as A_{cr}, at which the production of Br^- (inhibitor) in cell 1 due to the photochemical reactions is equal to the influx of Br^- due to the coupling. In Appendix B

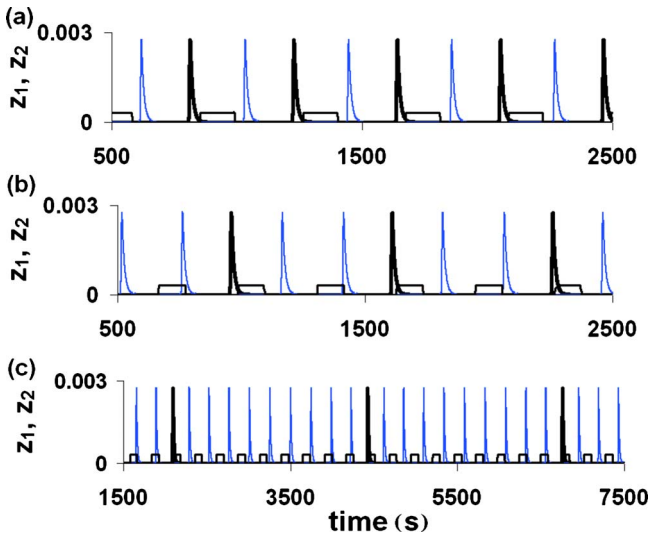

FIG. 7. (Color online) Examples of resonances (a) "1:1:1," (b) "1:2:2," and (c) "1:9:9" at $A=5\times10^{-4}$ and T_P/s=(a) 410, (b) 320, and (c) 260. Square waves are $400\times P_1(t)$. Concentrations of z_1 (black bold line) and z_2 (blue lighter line) are in units of mol/dm^3. All other parameters of models (1)–(9) as in Fig. 5.

we show how to evaluate A_{cr}. At k_f=1 s^{-1}, A_{cr} is in the range 3×10^{-4}–10^{-3} s^{-1}. So, we have three groups of resonances, one of which is associated with the intrinsic period T_0, and two others with the period of antiphase oscillation, T_C. These last two groups can emerge only in the case of inhibitory coupling, which generates new frequencies.

Examples of resonances 1:1:1, 1:2:2, and 1:9:9 at $A=5$ $\times10^{-4}$ s^{-1} with T_P between T_0 and T_C are shown in Fig. 7. The resonance 1:9:9 illustrates an interesting phenomenon, the dependence of the period T_{1_av} on T_P, which we refer to as frequency conversion, since an external frequency T_P^{-1} generates a signal with a new frequency $T_{1\_av}^{-1}$. Let us make a horizontal cross section of Fig. 5(a) at small $A=5$ $\times10^{-4}$ s^{-1}. The resulting doubled devil's staircase and sheaf resonances are shown in Fig. 8. The sheaf resonance in Fig. 8(b) reveals the anomalous dependence of T_{1_av} on T_P in the range of T_P between resonances 0:1:1 and 1:1:1. The period T_{1_av} decreases with T_P instead of increasing, as it does at large A. In the range $T_0<T_P<T_C$, oscillator 2 has average period T_{2_av} equal to T_P and $N_2=n$, while T_{1_av} increases as T_P approaches T_0 from above. Almost all resonances of the form $N_1:1:1$ ($N_1>1$) can be found. This phenomenon allows us to regulate T_{1_av} smoothly over a broad range of values. Due to this phenomenon we can think of our system of two inhibitorily coupled oscillators subject to periodic perturbation of one of them as a frequency transmitter or frequency converter.

The phenomenon of frequency conversion depends on the ratio T_C/T_0: the larger this ratio, the more profound the frequency conversion, and the tuning of T_{1_av} can be done more accurately. This behavior is illustrated in Fig. 9(a). Empirically, we find [Fig. 9(b)] that T_{1_av} is well approximated by

$$T_{1\_av} = c_1 + c_2 T_P^2/(T_P - T_0), \tag{11}$$

where the constants c_1 and c_2 depend on k_f (and consequently on T_C), A and probably on the parameters of the BZ

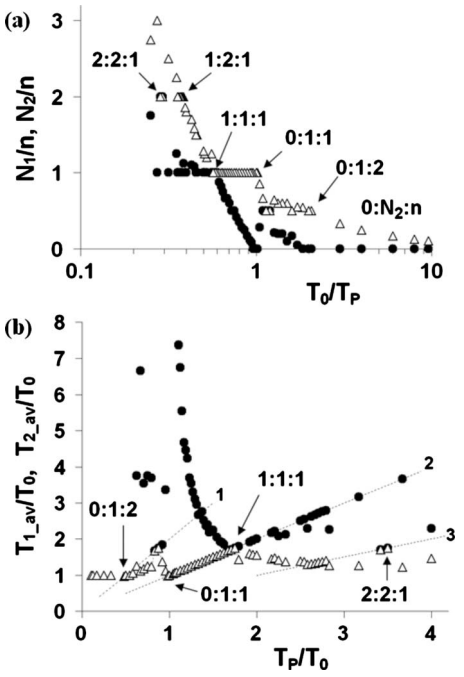

FIG. 8. (a) Doubled devil's staircase showing ratios N_1/n (black circles) and N_2/n (open triangles) as functions of T_0/T_P (T_0=240 s) with k_f=1 s^{-1} at amplitude $A=5\times10^{-4}$ s^{-1}. (b) Sheaf resonances. The same results as in (a), but in coordinates T_{1_av}/T_0-T_P/T_0 (black circles) and T_{2_av}/T_0-T_P/T_0 (open triangles); $T_{1\_av}=nT_P/N_1$ and $T_{2\_av}=nT_P/N_2$. Parameters as in Fig. 5. Slopes of dotted curves 1, 2, and 3 are 2, 1, and 1/2, respectively.

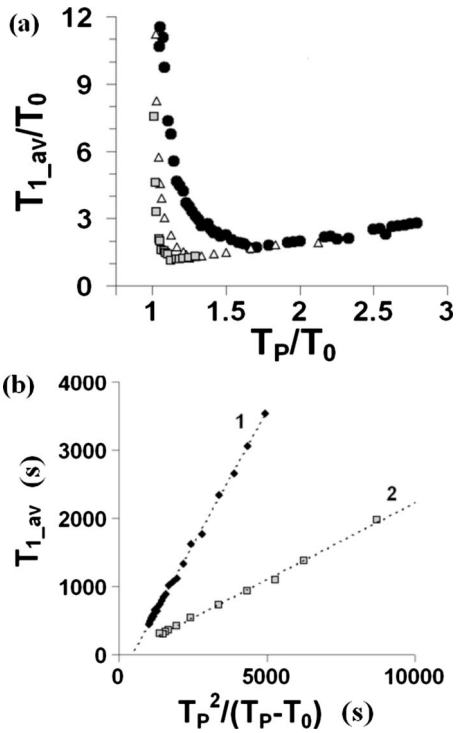

FIG. 9. (a) Dependence of T_{1_av}/T_0 on T_P/T_0 [as in Fig. 8(b)] at k_f=0.1 (squares), 0.2 (open triangles), and 1 (black circles). (b) Dependence of T_{1_av} on $T_P^2/(T_P-T_0)$ at k_f=1 (curve 1) and 0.2 (curve 2); $T_0<T_P<T_C$, T_0=240 s, and T_C=(curve 1) 385 s, (curve 2) 295 s.

reaction as well. Equation (11) gives us an analytical expression for frequency conversion from T_P^{-1} to $T_{1\_av}^{-1}$.

VI. DISCUSSION AND CONCLUSION

In the present work, we have found many new resonances in a system of two inhibitorily coupled BZ oscillators. Analogous results should be valid for other relaxation oscillators coupled via an inhibitor or by means of a signaling molecule (messenger) chemically linked to an inhibitor. A key feature of our model system is the ability of a messenger to affect the dynamics of oscillations. We expect that different messengers may result in different values of the coupling strength at which a particular resonance emerges. In general, the resonances found originate from the emergence of a new frequency T_C^{-1}, which in turn depends on the coupling strength. In a system of N identical oscillators coupled via an inhibitor, the number of new frequencies increases, depending on the geometry of coupling [25,32]. We may speculate that neurons in the brain utilize this feature for sensitive (resonant) perception of the external world. The sheaf resonances introduced in this work may be a convenient tool for describing such resonances in a system of N coupled oscillators.

Our finding of frequency conversion is in some sense analogous to the transformation of chemical signals (BZ waves) passing through a passive barrier [33–36]. If periodic BZ trigger waves (with frequency f_0) travel along a pseudo-1D stripe (for example, made of silica gel), in which a catalyst is immobilized, and reach a short gap of width l, in which there is no catalyst, these waves can continue propagating at the other end of the gap, but at a lower frequency f_P. The ratio f_P/f_0 depends on the width l. In our case the ratio T_{1_av}/T_0 depends on the period of external perturbation T_P. From a practical point of view, our configuration may be more convenient since it is easy to change T_P, while the width l of the gap is difficult to modify if the device is already fabricated.

Such a device might be used as a component in a chemical computer. By combining the inhibitory coupling described in this and other works [25] with the excitatory coupling associated with waves passing through a passive barrier, especially in combination with chemical diodes [34,37,38] that mimic unidirectional synaptic coupling in neurons, one may be able to develop a chemical device that brings us one step closer to modeling a real brain.

ACKNOWLEDGMENT

This work was supported by the National Science Foundation through Grant No. CHE-0526866.

APPENDIX A: COUPLING: PARTIAL VS ORDINARY DIFFERENTIAL EQUATIONS

Coupling between two water drops separated by an oil gap can be described by partial differential equations (PDE)

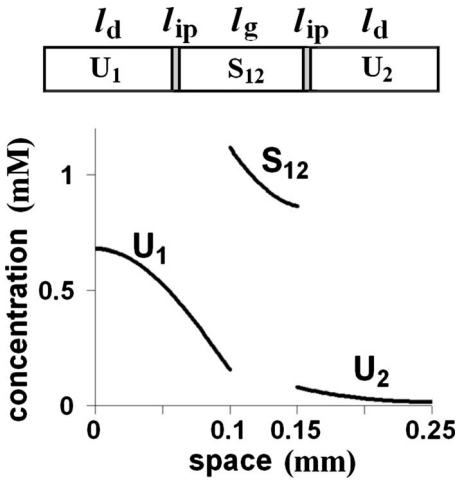

FIG. 10. Schematic drawing of two water droplets (width l_d) separated by an oil gap (width l_g) with thin interfaces (width l_{ip}) between them and a snapshot of the concentrations U_1, S_{12}, and U_2 obtained by solving the PDE at $l_d=0.01$ mm, $l_g=0.005$ mm, $l_{ip}=10^{-4}l_d$, $P_K=10$, initial concentrations $U_{1\_0}=10^{-3}M$, $S_{12\_0}=10^{-5}M$, and $U_{2\_0}=S_{12\_0}/P_K$ at $t=3$ s.

as well as ODE. The PDE description is more accurate but time-consuming; the ODE description is an approximation of the more realistic PDE model. To evaluate the quality of the ODE approximation, we compare these two approaches.

1. PDE

Consider a 1D model of two diffusively coupled cells or water drops of length l_d separated by an oil gap of length l_g (see Fig. 10). Bromine in the water drops is denoted as U_1 and U_2, while bromine in the oil drop is S_{12}. Suppose that the very thin interface between the water and the oil has thickness l_{ip}, which is sufficiently small that the final result is independent of l_{ip}. Simulations show that $l_{ip}/l_d<0.001$, $l_{ip}/l_g<0.001$ is sufficient to meet this requirement. In the narrow zone "l_{ip}" between drop 1 and the gap, the following very fast unimolecular "reactions" take place:

$$U_1 \rightarrow S_{12}, \quad k_{US}, \tag{A1}$$

$$S_{12} \rightarrow U_1, \quad k_{SU}. \tag{A2}$$

Analogous equations can be written for U_2 and S_{12}. The constants k_{US} and k_{SU} should be very large, and the final equilibrium between U_1, U_2, and S_{12} must be independent of these constants but dependent on their ratio

$$P_K = k_{US}/k_{SU}. \tag{A3}$$

At equilibrium, the uniform stationary concentrations of bromine soluble in water and in oil satisfy

$$P_K = [S_{12}]_{SS}/[U_1]_{SS} = [S_{12}]_{SS}/[U_2]_{SS}, \tag{A4}$$

where P_K is the partition coefficient. To model the diffusion of species U_1, S_{12}, and U_2 only in zones "left l_d+l_{ip}," "l_g+2l_{ip}," and "right l_d+l_{ip}," respectively, we set the diffusion coefficients as $D_{U_1}=D$ in zones "left l_d" and "left l_{ip}" and $D_{U_1}=0$ elsewhere; $D_{S_{12}}=D$ in zones "l_{ip}" and in zone "l_g" and $D_{S_{12}}=0$ elsewhere; the conditions for D_{U_2} are analogous to D_{U_1} but mirror symmetrical. To compare the kinetics obtained by solving these PDE and the corresponding ODE (below), we calculate the averaged values u_1, s_{12}, and u_2:

$$u_1 = \int_1 [U_1]/l_d \cong \int_{1'} [U_1]/(l_d + l_{ip}), \tag{A5}$$

$$s_{12} = \int_2 [S_{12}]/l_g \cong \int_{2'} [S_{12}]/(l_g + 2l_{ip}), \tag{A6}$$

$$u_2 = \int_3 [U_2]/l_d \cong \int_{3'} [U_2]/(l_d + l_{ip}), \tag{A7}$$

where the regions of integration "1" and "1′" in Eq. (A5) span from the lowest limit 0 corresponding to the left border of the left water droplet (see Fig. 10) to l_d and from 0 to l_d+l_{ip}, respectively; regions "2" and "2′" in Eq. (A6) go from l_d+l_{ip} to $l_d+l_{ip}+l_g$ and from l_d to $l_d+2l_{ip}+l_g$, respectively; regions "3" and "3′" in Eq. (A7) extend from $l_d+2l_{ip}+l_g$ to the largest limit $2l_d+2l_{ip}+l_g$ and from $l_d+l_{ip}+l_g$ to $2l_d+2l_{ip}+l_g$, respectively.

2. ODE

The ODE corresponding to the above problem can be written as

$$du_1/dt = -k_f u_1 + k_b s_{12}/r_V, \tag{A8}$$

$$ds_{12}/dt = r_V k_f u_1 - 2k_b s_{12} + r_V k_f u_2, \tag{A9}$$

$$du_2/dt = -k_f u_2 + k_b s_{12}/r_V. \tag{A10}$$

Summation of (A8)+(A9)/r_V+(A10) gives

$$d(u_1 + s_{12}/r_V + u_2)/dt = 0 \tag{A11}$$

or

$$u_1 + s_{12}/r_V + u_2 = C_0. \tag{A12}$$

The constant of integration C_0 can be found from the conservation of mass:

$$l_d u_1 + l_g s_{12} + l_d u_2 = M_0, \tag{A13}$$

where M_0 is the total mass. Equation (A12) follows from Eq. (A13) by dividing Eq. (A13) by l_d and $C_0=M_0/l_d$, $r_V=l_d/l_g$ (in 3D, $r_V=V_W/V_{oil}$, where V_W and V_{oil} are the volumes of the water droplet and the oil gap, respectively). The steady states $u_{1\_SS}=u_{2\_SS}\equiv u_{SS}$ and $s_{12\_SS}\equiv s_{SS}$ and the equilibrium relation (A14)

$$r_V k_f/k_b = P_K = u_{SS}/s_{SS} \tag{A14}$$

can be found from Eqs. (A8)–(A10) as

$$u_{SS} = C_0/(2 + k_f/k_b), \quad s_{SS} = P_K u_{SS}. \tag{A15}$$

Using Eq. (A12) and introducing new variables $u_1'=u_1-u_{SS}$, $s'=s_{12}-s_{SS}$, and $u_2'=u_2-u_{SS}$ into (A8)–(A10), we can reduce

the number of variables by one, since $s'=-r_V(u_1'+u_2')$:

$$du_1'/dt = -k_f u_1' - k_b(u_1' + u_2'), \tag{A16}$$

$$du_2'/dt = -k_f u_2' - k_b(u_1' + u_2'). \tag{A17}$$

Equations (A16) and (A17) can be solved analytically:

$$2u_1' = (u_{10}' - u_{20}')\exp(-\lambda_1 t) + (u_{10}' + u_{20}')\exp(-\lambda_2 t), \tag{A18}$$

$$2u_2' = -(u_{10}' - u_{20}')\exp(-\lambda_1 t) + (u_{10}' + u_{20}')\exp(-\lambda_2 t), \tag{A19}$$

where

$$\lambda_1 = k_f \quad \text{and} \quad \lambda_2 = k_f + 2k_b \tag{A20}$$

and u_{10}' and u_{20}' are the initial values of u_1' and u_2', respectively. Note that $s'=-r_V(u_{10}'+u_{20}')\exp(-\lambda_2 t)$, as follows from Eqs. (A18) and (A19), and therefore $\ln(-s')=\ln(-s_0')-\lambda_2 t$.

3. Comparison

To compare the processes of approaching the equilibria described by the PDE and ODE, we choose arbitrary initial conditions (shown in the caption to Fig. 10) and vary the parameters of the model: k_f, P_K, l_d, and l_g or r_V $(=l_d/l_g)$. The parameters P_K and r_V can be compared directly in the two approaches. Parameter k_f in the ODE approach is usually chosen in such a way that $k_f \cong D/l_d^2$ at $D=10^{-5}$ cm^2/s. However this is not necessary since any kinetics obtained at one value of k_f can be rescaled to the kinetics with another k_f by using the condition that $k_f t=$const. Parameter k_b in the ODE approach is determined from Eq. (A14). The analogous parameter in the PDE approach has to be determined from the result of simulations. In general, this can be done in several ways: (i) as $k_b=r_V k_1/P_K$, where k_1 is the slope of the curve $\ln(u_1')$ vs t at large t [slope 1 in Fig. 11(a)], since this slope should be equal to k_f; (ii) as $k_b=(k_2-k_f)/2$, where k_2 is the slope of curve $\ln(-s')$ vs t [slope 2 in Fig. 11(a)], since this slope should be equal to k_f+2k_b [see Eq. (A20)]; (iii) as a combination of methods (i) and (ii), for example, $k_b=k_2/(2+P_K/r_V)$. If the agreement of the PDE and ODE approaches is good, all methods give the same k_b, if not, then k_b obtained by different methods can differ significantly.

In Fig. 11 we show three examples of simulations: one example corresponds to relatively good agreement (when $r_V \cong 1$), while the other two illustrate poor agreement between the PDE and ODE approaches (when $r_V < 1$ and when $r_V \gg 1$ at $P_K \geq 1$). The ODE simulations of Eqs. (A8)–(A10) (right column in Fig. 11) give curves u_1', $-u_2'$ and $-s'$, the slopes of which in semi-logarithmic coordinates give λ_1 and λ_2 [see Eq. (A18)–(A20)]. The slopes of the analogous curves obtained by the PDE approach are marked as k_1 and k_2. The quality of the agreement between the PDE and ODE approaches can be assessed by comparing the ratios k_2/k_1 and λ_2/λ_1. If $k_2/k_1 \cong \lambda_2/\lambda_1$, then the ratios k_f/k_b are almost the same in the two approaches (at the same P_K and r_V) and the ODE approach should be satisfactory.

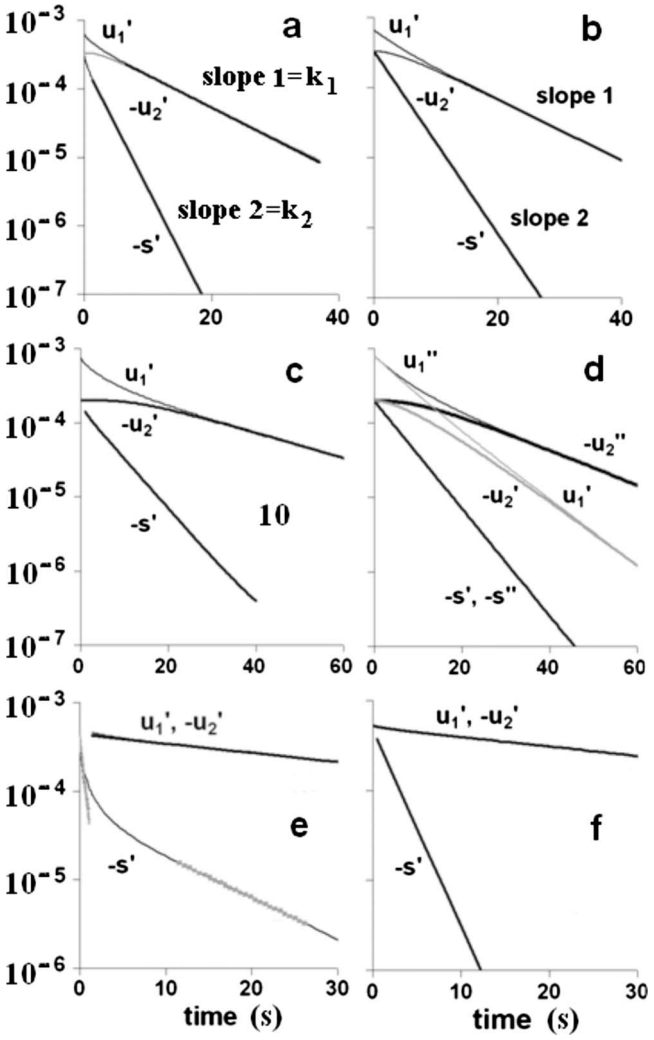

FIG. 11. Solutions obtained from PDE (left column) at $D=10^{-5}$ cm^2/s and from corresponding ODE (right column). For all ODE solutions, slope $1=\lambda_1=k_f$ [slope of curve $\ln(u_1')$ or curve $\ln(-u_2')$ vs t at large t] and slope $2=\lambda_2=k_f+2k_b$ [slope of curve $\ln(-s')$ vs t]. For all PDE solutions, slope 1 is marked as k_1 and slope 2 as k_2. (a) $l_d=l_g=0.01$ cm ($r_V=1$), $P_K=1$, $k_1=0.108$ s^{-1}, and $k_2=0.42$ s^{-1}; (b) $k_f=0.1$ s^{-1}, $r_V=1$, $P_K=1$, and $k_b=0.1$ s^{-1}; (c) $l_d=0.01$ cm, $l_g=0.03$ cm ($r_V=0.333$), $P_K=1$, $k_1=0.0395$ s^{-1}, and $k_2=0.16$ s^{-1}; (d) $k_f=0.1$ s^{-1}, $P_K=1$ for curves u_1', $-u_2'$, and $-s'$; $r_V=0.333$, $P_K/r_V=k_f/k_b$; for curves u_1'', $-u_2''$, and $-s''$ [Eqs. (A8″) and (A10″)]: $r_V'=0.666$, $P_K/r_V'=k_f/k_b$, curves $-s'$ and $-s''$ coincide. (e) $l_d=0.03$ cm, $l_g=0.003$ cm ($r_V=10$), $P_K=1$, $k_1=0.024$ s^{-1}, slope of curve $\ln(-s')$ vs t is 1.98 at small t and 0.107 (=slope 2) at large t, (f) $k_f=0.024$ s^{-1}, $r_V=10$, $P_K=1$, and $k_b=0.24$ s^{-1}.

In Fig. 12(a), we show how the ratio $(k_2/k_1)/(\lambda_2/\lambda_1)$ depends on r_V at different P_K. For $0.5<r_V<5$, the ratio $(k_2/k_1)/(\lambda_2/\lambda_1)$ is close to 1, and we conclude that the ODE approach can be used in this range. At large P_K, the acceptable range of r_V widens.

Analyzing the dependence of the slope k_1 on the parameters l_d, l_g and P_K, we obtain the relation between the constant k_f calculated from the PDE approach and the length of the water droplet l_d. This dependence is presented in Fig.

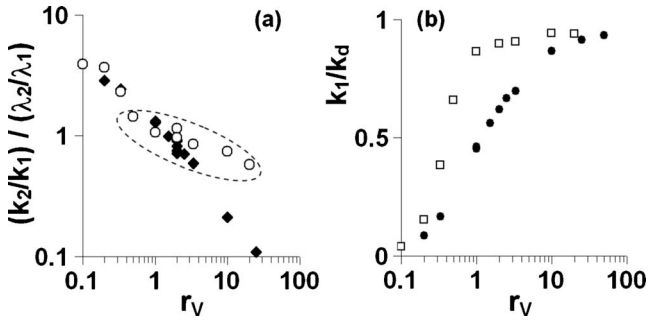

FIG. 12. (a) Relation between coupling parameters k_2/k_1 obtained by PDE and coupling parameters λ_2/λ_1 obtained by ODE as a function of r_V at different P_K. $P_K=10$ (open circles), 1 (black rhombs); (b) dependence of the coupling strength $k_1=k_f$ on r_V at different P_K. $P_K=10$ (open squares), 1 (black circles), and $k_d=2D/l_d^2$.

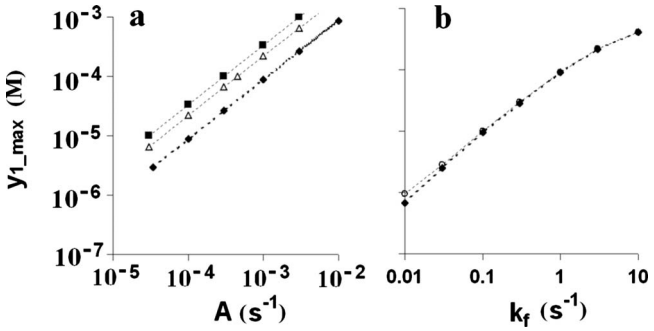

FIG. 13. Maximum amplitude y_{1_max} of oscillations of inhibitor in cell 1 without autocatalysis ($k_4=0$ in cell 1) due to (a) external periodic perturbation only (without cell 2) and (b) due to coupling only at $h=0.15M$, $a=0.3M$, $m=0.6M$, $c_0=0.003M$, and $k_b=r_V k_f/P_K$. The value of y_{1_min} (minimum amplitude) is significantly smaller than y_{1_max} (it may be several orders of magnitude smaller, depending on T_P) and is not shown. (a) $T_P/s=120$ (open triangles), 240 (black rhombs), 480 (black squares), $k_f=1$, $P_K=2.5$, $r_V=2$, (b) $r_V=2$ and 20 (almost coincident), $P_K=2.5$, $A=0$.

12(b), where k_d is the diffusion controlled rate constant, $k_d=2D/l_d^2$. With increasing r_V and P_K, k_f tends to k_d.

In general, we can write

$$k_f = k_d f(r_V, P_K), \tag{A21}$$

where $f(r_V, P_K)=1$, if r_V and/or P_K are large. Empirically we have found that satisfactory agreement between the PDE and ODE kinetics (in a broad range of r_V and P_K) can be obtained if

$$f(r_V, P_K) = r_V P_K/(1+r_V P_K). \tag{A22}$$

Using Eqs. (A14), (A21), and (A22), Eqs. (A8)–(A10) can be rewritten as follows:

$$du_1/dt = k_d r_V P_K(-u_1 + s_{12}/P_K)/(1+r_V P_K), \tag{A23}$$

$$ds_{12}/dt = k_d r_V^2 P_K(u_1 - 2s_{12}/P_K + u_2)/(1+r_V P_K), \tag{A24}$$

$$du_2/dt = k_d r_V P_K(-u_2 + s_{12}/P_K)/(1+r_V P_K). \tag{A25}$$

The discrepancy between the ODE and PDE approaches [seen, for example, in Figs. 11(c) and 11(d) as well as Figs. 11(e) and 11(f)] arises from the fact that k_b/k_f is proportional to $l_d/l_g(=r_V)$, as follows from Eq. (A14). On the other hand, k_f is related to $k_d=2D/l_d^2$ [as we see from Fig. 12(b)] or in other words, $k_f \propto 1/l_d^2$. From the kinetic point of view, the same should be true for k_b, $k_b \propto 1/l_g^2$. From this relationship, it follows that k_b/k_f should be proportional to l_d^2/l_g^2 rather than to l_d/l_g. Obviously, $l_d/l_g \cong l_d^2/l_g^2$ only when $l_d/l_g \cong 1$, and therefore we have good agreement between the two approaches when $l_d/l_g \cong 1$.

If l_g is very small and $l_d/l_g \gg 1$, then the time delay in communication between cells 1 and 2 can be ignored and the variable s_{12} eliminated through $s_{12}=r_V k_f(u_1+u_2)/(2k_b)$. Equations (A8) and (A10) are then modified as follows:

$$du_1/dt = k_f(u_2-u_1)/2, \tag{A8'}$$

$$du_2/dt = k_f(u_1-u_2)/2. \tag{A10'}$$

In this case $k_f \cong 1.25D/l_d^2$ (which results from solution of the corresponding PDE).

If $l_d/l_g \ll 1$, then the gap can be split into several equal parts approximately equal to l_d. For splitting into two parts, the ODE corresponding to Eqs. (A8)–(A10) are written as follows:

$$du_1/dt = -k_f u_1 + k_b s_1/r_{V'}, \tag{A8''}$$

$$ds_1/dt = r'_V k_f u_1 - k_b s_1 - k_{bf}(s_1 - s_2), \tag{A9'}$$

$$ds_2/dt = r'_V k_f u_2 - k_b s_2 - k_{bf}(s_2 - s_1), \tag{A9''}$$

$$du_2/dt = -k_f u_2 + k_b s_2/r'_V, \tag{A10''}$$

with $k_{bf}=k_b$ and $r'_V=2r_V$, $k_b=r'_V k_f/P_K$. In Fig. 11(d) we show the result of simulations of Eqs. (A8″) and (A10″) marked as $u''_1=u_1-u_{SS}$, $-u''_2=u_{SS}-u_2$, and $-s''=s_{SS}-(s_1+s_2)/2$. Such an approach may significantly improve the agreement.

APPENDIX B: ESTIMATION OF [Br^-] PRODUCED IN DROPLET 1 DUE TO (i) EXTERNAL PERIODIC PERTURBATION AND (ii) COUPLING

We can expect that the interaction between coupling with oscillator 2 and periodic perturbation directly affecting oscillator 1 is most complex when these effects are of comparable magnitude. To estimate the size of each of these perturbations of oscillator 1, we consider two cases: (i) periodic perturbation of oscillator 1 only (without the second oscillator) at $k_4=0$ in cell 1 and (ii) two coupled oscillators with $P(t)=0$ at $k_4=0$ in cell 1. In both cases we ignore the autocatalysis in cell 1 (putting $k_4=0$), which focuses the effect of perturbation or coupling on the concentration of inhibitor, y_1.

At the same parameters as used in Fig. 4, we have found the dependence (shown in Fig. 13) of the maximum ampli-

tude of oscillations of inhibitor y_1 due to periodic perturbation only and due to coupling to oscillatory cell 2 only at several k_f, r_V, A, and T_P. As can be seen in Fig. 13(b), at $k_f=1$ s^{-1}, $y_{1\_max}=9\times10^{-5}$ M. Approximately the same amplitudes y_{1_max} are obtained due to external periodic perturbation at $A=4.5\times10^{-4}$ s^{-1} and $T_P=120$ s, at $A=1\times10^{-3}$ s^{-1} and $T_P=240$ s, and at $A=3\times10^{-4}$ and $T_P=480$ s. It is exactly in this range of $A=3\times10^{-4}-10^{-3}$ s^{-1} that the resonance tongues in Fig. 13 drastically change their width.

[1] *Oscillations and Traveling Waves in Chemical Systems*, edited by R. J. Field and M. Burger (Wiley, New York, 1985).

[2] I. R. Epstein and J. A. Pojman, *An Introduction to Nonlinear Chemical Dynamics* (Oxford University Press, New York, 1998).

[3] Y. Kuramoto, *Chemical Oscillations, Waves, and Turbulence* (Springer, Berlin, 1984).

[4] A. Pikovsky, M. Rosenblum, and J. Kurths, *Synchronization: A Universal Concept in Nonlinear Sciences* (University Press, Cambridge, 2001).

[5] G. V. Osipov, J. Kurths, and C. Zhou, *Synchronization in Oscillatory Networks* (Springer, Berlin, 2007).

[6] M. F. Crowley and I. R. Epstein, J. Phys. Chem. **93**, 2496 (1989).

[7] M. Dolnik and I. R. Epstein, Phys. Rev. E **54**, 3361 (1996).

[8] G. B. Ermentrout and N. Kopell, SIAM J. Appl. Math. **50**, 125 (1990).

[9] A. Koseska, E. Volkov, A. Zaikin, and J. Kurths, Phys. Rev. E **76**, 020901 (2007).

[10] H. G. Rotstein and R. Kuske, Physica D **215**, 46 (2006).

[11] M. Brøns, P. Gross, and K. Bar-Eli, Int. J. Bifurcation Chaos Appl. Sci. Eng. **7**, 2621 (1997).

[12] M. Dolnik and M. Marek, J. Phys. Chem. **92**, 2452 (1988).

[13] M. Dolnik and I. R. Epstein, J. Chem. Phys. **97**, 3265 (1992).

[14] G. Markman and K. Bar-Eli, J. Phys. Chem. **98**, 12248 (1994).

[15] G. Markman, V. Vasilchenko, S. Markman, and K. Bar-Eli, Math. Comput. Modell. **31**, 143 (2000).

[16] O. Pešek, P. Kaspar, L. Schreiberová, and I. Schreiber, J. Phys. Chem. A **108**, 2436 (2004).

[17] T. Okano and K. Miyakawa, Phys. Rev. E **80**, 026215 (2009).

[18] A. F. Taylor *et al.*, Science **323**, 614 (2009).

[19] P. C. Bressloff and S. Coombes, Neural Comput. **12**, 91 (2000).

[20] M. I. Rabinovich, P. Varona, A. I. Selverston, and H. D. I. Abarbanel, Rev. Mod. Phys. **78**, 1213 (2006).

[21] D. V. Senthilkumar, J. Kurths, and M. Lakshmanan, Chaos **19**, 023107 (2009).

[22] E. I. Volkov, E. Ullner, A. A. Zaikin, and J. Kurths, Phys. Rev. E **68**, 061112 (2003).

[23] E. I. Volkov, M. N. Stolyarov, A. A. Zaikin, and J. Kurths, Phys. Rev. E **67**, 066202 (2003).

[24] E. M. Izhikevich, *Dynamical Systems in Neuroscience: The Geometry of Excitability and Bursting* (MIT Press, Cambridge, 2007).

[25] M. Toiya, V. K. Vanag, and I. R. Epstein, Angew. Chem., Int. Ed. **47**, 7753 (2008).

[26] B. P. Belousov, *Collection of Short Papers on Radiation Medicine* (Medgiz, Moscow, 1959), p. 145.

[27] A. M. Zhabotinsky, Proc. Acad. Sci. USSR **157**, 392 (1964).

[28] V. K. Vanag and I. R. Epstein, J. Chem. Phys. **131**, 104512 (2009).

[29] R. J. Field, E. Körös, and R. M. Noyes, J. Am. Chem. Soc. **94**, 8649 (1972).

[30] S. Kádár, T. Amemiya, and K. Showalter, J. Phys. Chem. A **101**, 8200 (1997).

[31] D. V. Ramana Reddy, A. Sen, and G. L. Johnston, Phys. Rev. Lett. **80**, 5109 (1998).

[32] M. Toiya *et al.*, J. Chem. Phys. Lett. **1**, 1241 (2010).

[33] G. R. Armstrong, A. F. Taylor, S. K. Scott, and V. Gaspar, Phys. Chem. Chem. Phys. **6**, 4677 (2004).

[34] J. N. Gorecka, J. Gorecki, and Y. Igarashi, J. Phys. Chem. A **111**, 885 (2007).

[35] J. Gorecki, J. N. Gorecka, K. Yoshikawa, Y. Igarashi, and H. Nagahara, Phys. Rev. E **72**, 046201 (2005).

[36] J. Sielewiesiuk and J. Gorecki, Phys. Rev. E **66**, 016212 (2002).

[37] J. N. Gorecka, J. Gorecki, and Y. Igarashi, Int. J. Unconv. Comput. **5**, 129 (2009).

[38] K. Agladze, R. R. Aliev, T. Yamaguchi, and K. Yoshikawa, J. Phys. Chem. **100**, 13895 (1996).